AIAA JOURNAL
Vol. 32, No. 9, September 1994

Static Shape Control for Adaptive Wings

Fred Austin,* Michael J. Rossi,† William Van Nostrand,‡ and Gareth Knowles§
Grumman Corporate Research Center, Bethpage, New York 11714
and
Antony Jameson¶
Princeton University, Princeton, New Jersey 08544

A theoretical method was developed, and experimentally validated, to control the static shape of flexible structures by employing internal translational actuators. A finite element model of the structure, without the actuators present, is employed to obtain the multiple-input, multiple-output control-system gain matrices for actuator-load control as well as actuator-displacement control. The method is applied to the quasistatic problem of maintaining an optimum-wing cross section during various transonic-cruise flight conditions to obtain significant reductions in the shock-induced drag. Only small, potentially achievable, adaptive modifications to the profile are required. The adaptive-wing concept employs actuators as truss elements of active ribs to reshape the wing cross section by deforming the structure. Finite element analyses of an adaptive-rib model verify the controlled-structure theory. Experiments on the model were conducted, and arbitrarily selected deformed shapes were accurately achieved.

Introduction

SHAPE control of flexible structures has the potential to improve aerodynamic and hydrodynamic lifting-surface performance, to reduce drag on submersible components, and to correct errors on optical, radar, and IR reflectors. We develop a general method for static shape control of structures and discuss its potential for adaptive wings.

Adaptive wings with variable leading- and trailing-edge devices have been studied to enhance maneuvers, to reduce the critical root-bending moment, to reduce drag, and to improve gust-alleviating response.[1,2] Unlike these studies, we are exploring adaptive wings to improve aircraft performance during transonic cruise, a problem that requires smaller shape changes, but primarily in the region between the leading and trailing edges.[3,4] The shock-induced drag can be reduced dramatically during transonic cruise if the airfoil has the correct shape. Wings that are optimized for a single cruise condition, therefore, usually have high drag at other cruise conditions. However, by adaptively modifying the wing cross section, it is possible to maintain optimum performance as the flight condition changes. It will be seen that the required shape changes are small and therefore potentially achievable.

In our previous work,[3] we developed a procedure to compute the adaptive-structure control-system gain matrix; however, the method required the inverse of the stiffness matrix of the structure with the actuators removed. In some designs, when the actuators are removed, the structure becomes a linkage or becomes disconnected, and, consequently, the stiffness matrix becomes semidefinite and cannot be inverted. A method that does not require the inverse of the system stiffness matrix was developed later.[4] Open-loop experiments validated the method of developing the gain matrix. In these previous studies, when there were insufficient actuators to accurately achieve the desired shape, the solution that was developed minimized the error in the equation relating the actuator loads to the desired shape. In the current study, solutions are developed that minimize the error between the desired and achievable shapes. Also, closed-loop control is required for increased accuracy and for performing shape control in the presence of unmeasured external loads, such as air loads. Early closed-loop control studies provided evidence that accurate shapes could be achieved in the presence of external loads.[5] In addition to new analytical results, this paper contains a more complete set of open- and closed-loop experimental measurements.

Shape Control of Flexible Structures

As shown in Fig. 1, the concept employs one or more flexible surfaces, which could be curved, separated by translational actuators and possibly other structural members. The variables used in the structural analysis and their coordinate systems are shown in Fig. 2, $\boldsymbol{x}'$ and $\boldsymbol{f}'$ are the deformations and forces on the structure, respectively, in the global coordinate system. A finite element model of the structure, without the actuators, is developed to obtain the system stiffness matrix $\boldsymbol{K}'$. The actuators are represented by the loads that they exert on the structure. The structural equations are

$$\boldsymbol{K}'\boldsymbol{x}' = \boldsymbol{f}'_a + \boldsymbol{f}'_e \tag{1}$$

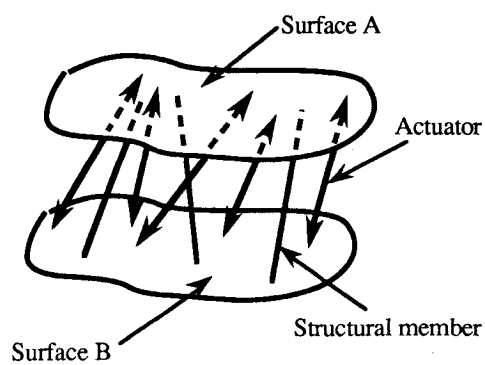

Fig. 1 General structure.

Received Oct. 14, 1993; revision received April 4, 1994; accepted for publication April 4, 1994.

*Senior Staff Scientist, Controls and Dynamics Theory Laboratory.
†Senior Research Scientist, Controls and Dynamics Theory Laboratory.
‡Research Engineer, Controls and Dynamics Theory Laboratory.
§Laboratory Head, Controls and Dynamics Theory Laboratory.
¶James S. McDonnell Distinguished University Professor of Aerospace Engineering, Olden Street, Engineering Quadrangle. Fellow AIAA.

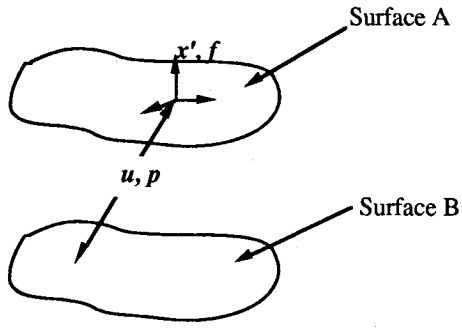

Fig. 2 General structure with global and actuator coordinate systems.

where the loads have been separated into f'_a, a vector of the actuator loads, and f'_e, a vector of aerodynamic and, possibly, other external loads.

If p is a vector of the actuator loads along the actuators, taken as positive when the actuators are in compression and pushing against the structure, then

$$f'_a = T'p \tag{2}$$

where T' contains the direction cosines of the actuator loads as well as information specifying that the actuator loads are applied to the structure in equal and opposite pairs. Since virtual work is conserved,

$$u = T'^T x' \tag{3}$$

where u is a vector containing the extensions of each actuator.

Next, we select a new set of independent coordinates $x = [x_1\ x_2]^T$, where x_1 contains the coordinates that will be used to define the desired shape, and x_2 contains the remaining coordinates to form the independent set. For example, if the structure has curved surfaces, x_1 could contain coordinates that are normal to the surface, and x_2 could contain coordinates that are tangential to the surface as well as rotational coordinates that may not be required to define the shape. A matrix G can be formed to transform the vectors from one coordinate system to the other; i.e.,

$$x' = Gx = [G_1\ G_2]\begin{bmatrix} x_1 \\ x_2 \end{bmatrix} \tag{4}$$

Equation (4) is used to transform Eqs. (1–3), and the results are

$$Kx = f_a + f_e \tag{5}$$

$$f_a = Tp \tag{6}$$

$$u = T^T x \tag{7}$$

where

$$K = G^T K' G \tag{8}$$

$$f_a = G^T f'_a \quad \text{and} \quad f_e = G^T f'_e \tag{9}$$

$$T = G^T T' \tag{10}$$

From Eqs. (5) and (6),

$$\begin{bmatrix} K_{11} & K_{12} \\ K_{21} & K_{22} \end{bmatrix}\begin{bmatrix} x_1 \\ x_2 \end{bmatrix} = \begin{bmatrix} T_1 \\ T_2 \end{bmatrix} p + \begin{bmatrix} f_{e1} \\ f_{e2} \end{bmatrix} \tag{11}$$

where the partitioning of K, T, and f_e is consistent with the partitioning of x. K_{22} is the stiffness matrix of the structure when the coordinates x_1, corresponding to the points used to describe the shape, are held. In practical cases, these extra supports are sufficient to eliminate any semidefinite property of the structure with the actuators removed; therefore, K_{22} can be inverted. The second of the equations implied in Eq. (11) is solved for x_2, and the result is

$$x_2 = K_{22}^{-1}(T_2 p - K_{21}x_1 + f_{e2}) \tag{12}$$

This equation is substituted into the first of the equations implied in Eq. (11) to obtain

$$\bar{T}p = \bar{K}x_1 - \bar{f}_e \tag{13}$$

where

$$\bar{T} = T_1 - K_{12}K_{22}^{-1}T_2 \tag{14}$$

$$\bar{K} = K_{11} - K_{12}K_{22}^{-1}K_{12}^T \tag{15}$$

$$\bar{f}_e = f_{e1} - K_{12}K_{22}^{-1}f_{e2} \tag{16}$$

$\bar{K}$ is the stiffness matrix relating the coordinates x_1 to the actuator and external loads. If these loads are given, x_1 is uniquely determined in practical structures; therefore $\bar{K}$ is invertible.

Often, $\bar{T}$ is not invertible. In fact, generally the number of actuators will not be equal to the number of components in the shape vector x_1; consequently, $\bar{T}$ may not even be square. We develop control laws by obtaining solutions that minimize a measure of the surface error $\|x_1 - x_{1d}\|$ where x_{1d} is the desired value of x_1 and the double bars indicate the 2 norm, i.e., the square root of the sum of the squares of the components. Either actuator loads or actuator displacements can be controlled.

To effectively employ open-loop control, the loads must be known, and the finite element model of the system must be sufficiently accurate. Closed-loop control does not require a knowledge of the loads, and results in more accurate shapes.

Open-Loop Control

Actuator-Load Command

Equation (13) is solved for x_1. The result is

$$\bar{K}^{-1}\bar{T}p + \bar{K}^{-1}\bar{f}_e = x_1 \tag{17}$$

x_{1d}, the desired value of x_1, is subtracted from both sides to obtain

$$\bar{K}^{-1}\bar{T}p - (x_{1d} - \bar{K}^{-1}\bar{f}_e) = x_1 - x_{1d} \tag{18}$$

To minimize $\|x_1 - x_{1d}\|$,

$$p_d = V_f x_{1d} - V_f \bar{K}^{-1}\bar{f}_e \tag{19}$$

where p_d is the desired actuator-load vector and

$$V_f = (\bar{K}^{-1}\bar{T})^{\dagger} \tag{20}$$

where the dagger indicates the Moore-Penrose generalized inverse, which has the following properties.[6] When the number of actuators (dimension of p) is equal to the number of specified surface displacements (dimension of x_1), $\bar{K}^{-1}\bar{T}$ is square. If it is also nonsingular, the generalized inverse becomes the conventional inverse, and an exact solution ($x_1 = x_{1d}$) can be obtained. When there are fewer actuators than specified displacements, or when there are excess actuators and $\bar{K}^{-1}\bar{T}$ does not have full row rank, Eq. (19) provides the solution that minimizes $\|x_1 - x_{1d}\|$. When there are excess actuators and $\bar{K}^{-1}\bar{T}$ has full row rank, x_{1d} can be achieved exactly with many values of p; i.e., p is not unique. In this case, the solution given by Eq. (19) is the one that also minimizes $\|p\|$.

Actuator-Displacement Command

If actuator displacements are commanded instead of actuator loads, the actuator-displacement commands are obtained by the

following procedure. First, Eq. (7) is partitioned, Eq. (12) is substituted into the result, and Eq. (14) is used to obtain

$$\boldsymbol{u} = \bar{\boldsymbol{T}}^T \boldsymbol{x}_1 + \boldsymbol{T}_2^T \boldsymbol{K}_{22}^{-1} (\boldsymbol{T}_2 \boldsymbol{p} + \boldsymbol{f}_{e2}) \tag{21}$$

The actuator load vector $\boldsymbol{p}$ is set to the desired value $\boldsymbol{p}_d$ in this equation and Eq. (13), and the result is

$$\boldsymbol{u}_d = \bar{\boldsymbol{T}}^T \boldsymbol{x}_{1f} + \boldsymbol{T}_2^T \boldsymbol{K}_{22}^{-1} (\boldsymbol{T}_2 \boldsymbol{p}_d + \boldsymbol{f}_{e2}) \tag{22}$$

$$\bar{\boldsymbol{T}} \boldsymbol{p}_d = \bar{\boldsymbol{K}} \boldsymbol{x}_{1f} - \bar{\boldsymbol{f}}_e \tag{23}$$

where $\boldsymbol{x}_{1f}$ is the best-fit solution to $\boldsymbol{x}_{1d}$, and $\boldsymbol{u}_d$ is the desired value of $\boldsymbol{u}$. Next, Eq. (19) is substituted into Eqs. (22) and (23), and $\boldsymbol{x}_{1f}$ is eliminated from the resulting two equations to obtain the desired actuator command:

$$\boldsymbol{u}_d = \boldsymbol{H}_g \boldsymbol{x}_{1d} + \boldsymbol{u}_g \tag{24}$$

where

$$\boldsymbol{H}_g = (\bar{\boldsymbol{T}}^T \bar{\boldsymbol{K}}^{-1} \bar{\boldsymbol{T}} + \boldsymbol{T}_2^T \boldsymbol{K}_{22}^{-1} \boldsymbol{T}_2) \boldsymbol{V}_f \tag{25}$$

$$\boldsymbol{u}_g = (\bar{\boldsymbol{T}}^T - \boldsymbol{H}_g) \bar{\boldsymbol{K}}^{-1} \bar{\boldsymbol{f}}_e + \boldsymbol{T}_2^T \boldsymbol{K}_{22}^{-1} \boldsymbol{f}_{e2} \tag{26}$$

Closed-Loop Control

Actuator-Load Error

Equation (13) is subtracted from Eq. (23) to obtain

$$\bar{\boldsymbol{T}} (\boldsymbol{p}_d - \boldsymbol{p}) = \bar{\boldsymbol{K}} (\boldsymbol{x}_{1f} - \boldsymbol{x}_1) \tag{27}$$

This equation is solved for $\boldsymbol{x}_{1f}$, and $\boldsymbol{x}_{1d}$ is subtracted from both sides of the result, yielding

$$\bar{\boldsymbol{K}}^{-1} \bar{\boldsymbol{T}} (\boldsymbol{p}_d - \boldsymbol{p}) - (\boldsymbol{x}_{1d} - \boldsymbol{x}_1) = \boldsymbol{x}_{1f} - \boldsymbol{x}_{1d} \tag{28}$$

To minimize, $\| \boldsymbol{x}_{1f} - \boldsymbol{x}_{1d} \|$

$$\boldsymbol{p}_d - \boldsymbol{p} = \boldsymbol{V}_f (\boldsymbol{x}_{1d} - \boldsymbol{x}_1) \tag{29}$$

This equation is independent of external loads and is the desired feedback relation for closed-loop actuator-load control. When there are redundant actuators and the desired shape can be achieved exactly, Eq. (29) also provides the actuator loads that are closest to the desired loads; i.e., $\| \boldsymbol{p}_d - \boldsymbol{p} \|$ is minimized.

Actuator-Displacement Error

From Eqs. (21) and (22),

$$\boldsymbol{u}_d - \boldsymbol{u} = \bar{\boldsymbol{T}}^T (\boldsymbol{x}_{1f} - \boldsymbol{x}_1) + \boldsymbol{T}_2^T \boldsymbol{K}_{22}^{-1} \boldsymbol{T}_2 (\boldsymbol{p}_d - \boldsymbol{p}) \tag{30}$$

Equation (27) is solved for $\boldsymbol{x}_{1f} - \boldsymbol{x}_1$, and the result is substituted into Eq. (30) to obtain

$$\boldsymbol{u}_d - \boldsymbol{u} = (\bar{\boldsymbol{T}}^T \bar{\boldsymbol{K}}^{-1} \bar{\boldsymbol{T}} + \boldsymbol{T}_2^T \boldsymbol{K}_{22}^{-1} \boldsymbol{T}_2) (\boldsymbol{p}_d - \boldsymbol{p}) \tag{31}$$

Equation (29) is substituted into Eq. (31), and the result is

$$\boldsymbol{u}_d - \boldsymbol{u} = \boldsymbol{H}_g (\boldsymbol{x}_{1d} - \boldsymbol{x}_1) \tag{32}$$

which is the desired feedback relation for closed-loop actuator-displacement control.

Desired Airfoil Shapes

To assess the potential payoff from a variable wing structure, it is necessary to identify the critical operating conditions under which shape modifications might significantly improve the aerodynamic performance and the range of shape variations that might be needed. During the last several years, Jameson[7,8] has investigated the feasibility of using control theory to formulate the problem of optimum aerodynamic design. This has led to a new design method that merges concepts and techniques from computational fluid dynamics and control theory.

The key ideas are as follows. Suppose that the performance is measured by a cost function I. For example, to optimize a wing section, one might take

$$I = \alpha_1 \int_S (p - p_D)^2 \mathrm{d}S + \alpha_2 C_D \tag{33}$$

where p is the surface pressure, p_D is the desired surface pressure, and the integral is over the surface, while C_D is the drag coefficient, and α_1 and α_2 are weighting coefficients. Suppose now that the shape is defined by a function $f(x)$. Then one wishes to calculate the gradient or Frechet derivative $g = \partial I / \partial f$, such that if a change δf is made in f, then the first-order change in I is $\delta I = \int_S g \delta f \, \mathrm{d}S$. If one sets $\delta f = -\lambda g$, where λ is sufficiently small and non-negative, then

$$\delta I = -\int \lambda g^2 \, \mathrm{d}S < 0 \tag{34}$$

so an improvement is guaranteed unless $g = 0$, which is the condition for an optimum. Although g is the derivative in function space of an infinite-dimensional vector f, it can be calculated indirectly by solving an adjoint problem, at a cost about equal to that of a flow situation.[8] Thus, successive improvements towards the optimum can be made with iterations, each of which has a computational cost of about two flow solutions.

This method has been implemented with the transonic potential flow equation[8] and was used in the present study to develop optimum wing sections for a fighter aircraft at different design points. The simplification that results from the use of the nonlinear potential flow model makes it possible to perform the design calculations rapidly enough to allow a range of alternatives to be examined. Each calculation can be performed in about 10 min on an IBM RS 6000 model 530 workstation. To check the validity of the results, we evaluated the performance of each design by calculating the solution of the Euler equations for a range of transonic conditions.

A hypothetical fixed-wing version of the F-14 aircraft was selected as an example for this study. The choice of representative design points for the wing section is complicated by the fact that the actual F-14 wing has variable sweepback, which is normally adjusted to keep the effective Mach number and angle of attack in a range within which the existing section is quite efficient. An examination of the currently used program for sweep variation indicated that the most likely opportunity for improvement is in the transonic regime with the aircraft operating at a high subsonic Mach number with high lift and low sweep. A representative cruise condition is Mach 0.73 at 28-deg sweep with a lift coefficient $C_L = 0.65$. According to the simple theory of sweepback for a wing of infinite span, these are equivalent to a two-dimensional condition of Mach 0.69 with $C_L = 0.85$. This was taken as one design point, labeled "Y" in the study. The existing section already has a significant shock-induced drag of 39 counts ($C_D = 0.0039$) in this condition.

The design method was used to try to minimize C_D at the design point while simultaneously minimizing the change in the subsonic pressure distribution at Mach 0.2 to make the shape changes as small as possible. To prevent the design method from producing sections that are undesirably thin, an additional penalty for reduction of the contained volume was included in the cost function. Also, the initial section from which the optimization was started was thickened. In this way a number of sections of varying thicknesses were obtained, these being labeled F-14Y, F-14YT, F-14YU, and F-14YV in ascending order of thickness. Euler calculations verify that the shock-induced drag can be reduced to values of 5 to 7 counts at the design point, the thickness may also be slightly increased.

To examine the influence of modifications in the design point, a second point "X" was then selected with a slightly higher Mach

Table 1 Shock-induced drag

Design point X	$M = 0.72$,	$C_L = 0.75$	
Design point Y	$M = 0.69$,	$C_L = 0.85$	
Airfoil		C_D	
Designation	Series	Point X	Point Y
F-14X	Nominal	0.0007	0.0033[a]
F-14XT	Thick	0.0010	0.0032[a]
F-14XU	Thicker	0.0007	0.0034[a]
F-14XV	Thickest	0.0008	0.0036[a]
F-14Y	Nominal	0.0068[a]	0.0006
F-14YT	Thick	0.0061[a]	0.0005
F-14YU	Thicker	0.0041[a]	0.0006
F-14YV	Thickest	0.0037[a]	0.0007

[a]Off-design condition.

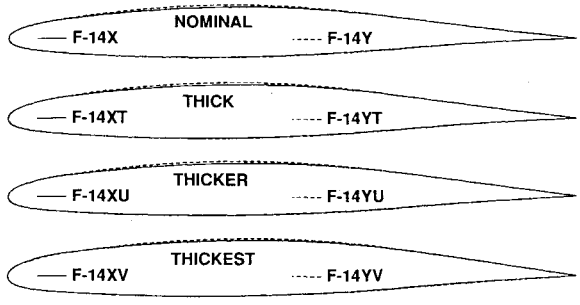

Fig. 3 Optimum wing cross sections for two design points.

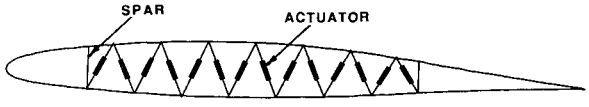

Fig. 4 Use of adaptive truss for wing rib.

number and lower lift coefficient, Mach 0.72 and $C_L = 0.75$. The same optimization procedure was used to produce another sequence of designs, F-14X, F-14XT, F-14XU, and F-14XV, again in ascending order of thickness. The existing F-14 section has a shock-induced drag coefficient of 75 counts in this condition. Again it was verified with Euler calculations that the shock-induced drag could be reduced to values of 7 to 10 counts without reducing the thickness.

Key results are shown in Table 1. The four airfoils beginning with the designation F-14X have been optimized for the X design point, and the four airfoils beginning with the designation F-14Y have been optimized for the Y design point. The drag is shown at the design point for which the airfoil has been optimized as well as for the other design point. For each of these optimum airfoils, it is seen that the drag is significantly higher at the off-design point and is reduced to moderate levels at the design point. The airfoils in each series can be potentially modified from one to the other by adaptive control; i.e., the F-14X airfoil can be modified into the F-14Y airfoil, the F-14XT airfoil can be modified into the F-14YT airfoil, etc. The most desirable pair seemed to be the F-14XU and F-14YU since they are slightly thicker than the existing F-14 section and have approximately the same drag as the thinner F-14X and F-14Y airfoils. Additional thickness might be used to advantage to reduce structure weight or to increase the wing span, which reduces the drag induced due to lift. As shown in Fig. 3, the required shape changes for each of the four series (nominal, thick, thicker, and thickest) are small and are, therefore, potentially achievable. Consequently, it appears possible that as flight conditions change, adaptive variation of the wing cross section could enable the optimum section to be used continuously to dramatically reduce the shock-induced drag, thereby extending the transonic cruise envelope.

Test Article

One method of implementing the shape-control concept for an adaptive wing is to incorporate active trusses in the wing-rib structure (Fig. 4). The diagonal elements are translational actuators that expand and contract to deform the airfoil. We constructed a model of an adaptive rib with 14 actuators to demonstrate the shape-control concept (Figs. 5 and 6). The model is approximately 4 ft wide and 10 in. high. The upper and lower caps are aluminum with T-shaped cross sections (3 in. wide, 0.050 in. thick, with 0.50 × 0.25 in. ribs). In the undeformed condition, the upper and lower surfaces are flat. Fourteen actuators are used to form the truss structure. No attempt was made to optimize the actuators. Terfenol-based magnetostrictive actuators and hydraulic actuators, as well as other devices, are being considered; however, in our model, mechanical ball-screw actuators are used since they are relatively inexpensive and available.

A set of internal linear variable-displacement transformers (LVDTs) (Fig. 6) measure the actuator displacements, and external LVDTs (Fig. 7) measure both the upper and lower surface displacements. External loads can be applied to one surface through cables

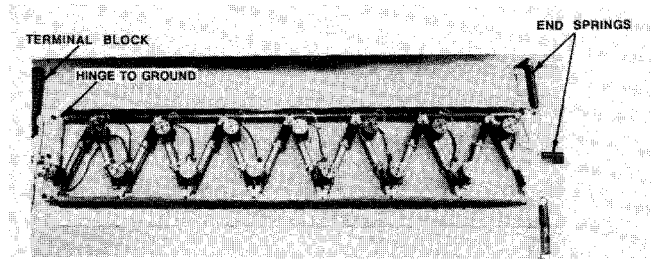

Fig. 5 Adaptive rib test article.

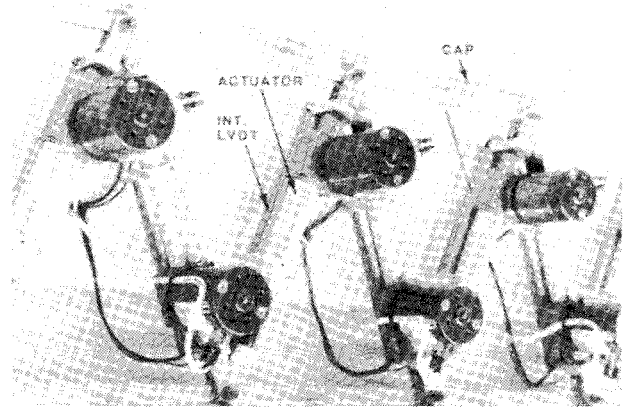

Fig. 6 Detail of actuators and LVDTs.

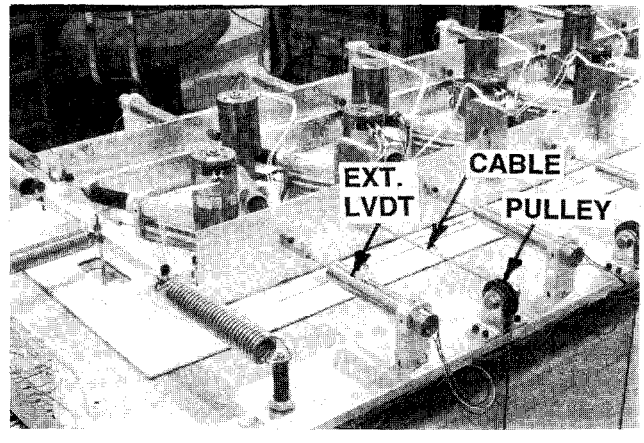

Fig. 7 Surface displacement sensors and load-application devices.

that are guided over pulleys and loaded with lead weights (Figs. 7 and 8). Each of the weights shown is approximately 26.5 lb.

Finite Element Analysis

A finite element (FE) model, containing 206 beam elements and 30 triangular-membrane elements (Fig. 9), was developed by employing the Grumman Automated STRuctural AnaLysis (ASTRAL) COmprehensive Matrix Algebra Program (COMAP) finite element (FE) system. The structure is pin connected at points A and B and spring connected to ground at point C in the x, y, and θ directions to represent spar flexibility. Actuator loads to achieve commanded shapes of the unloaded structure were computed by using Eq. (19). The actuator loads were then applied to the FE model, and the deformations were computed. Since the 14 transverse displacements of the actuator joints were selected to define the surface shapes, and there are also 14 actuators, the generalized inverse, Eq. (20), is identical to the conventional inverse, and we were able to achieve deflections of the joints exactly. Some of the deformed shapes obtained are illustrated in Fig. 10. The bottom-surface deflections in Figs. 10b and 10c, at first, seem counterintuitive since the loads applied to the surfaces by each actuator must be equal and opposite but the surfaces do not deform in opposing directions. However, it is easy to verify that the resultant of the loads applied at each vertex by the actuators that contact it can have a vertical component that is zero or upward at each lower vertex as well as at each upper vertex, even though the loads applied by each actuator are equal and opposite. Racking (Fig. 10d) is one method of achieving wing twist.

Control System

A nonlinear finite element analysis of the model shows that, with actuator-load control, nonlinear effects can produce up to 8% errors in the surface for the camber deformation shown in Fig. 10c. Consequently, actuator deflection control, which we believe will produce far more accurate deformations than load control, has been selected to achieve desired upper and lower rib-surface shapes. A flow diagram illustrating the control concept is shown in Fig. 11. Fourteen inner control loops (not shown) employ rate and velocity feedback to control each actuator.

To limit the dynamic response, the shape-change commands were varied gradually from the current shape to the desired shape over a 5-s period according to a one minus cosine waveform. Both open- and closed-loop control experiments were performed.

In the open-loop experiments, external loads were not applied since these loads are not measured, and in this case, it is not possible to achieve desired shapes in the presence of unknown loads. Desired shapes were commanded and multiplied by the gain matrix $\boldsymbol{H}_g$ to obtain the corresponding actuator lengths in accordance with Eq. (24). Then each actuator was commanded to assume its computed length. Actuator lengths were measured with the internal LVDTs, and actuator-length errors were corrected; i.e., the loop around each actuator was closed so that its commanded length could be achieved relatively accurately. To evaluate the accuracy of the gain matrix, surface shape was measured with the external LVDTs, but surface errors were not corrected; therefore, the overall loop was open.

In the closed-loop experiments, unmeasured external loads were applied and the external LVDTs sensed the rib shape. The surface error was multiplied by the gain matrix $\boldsymbol{H}_g$ to determine and correct the actuator stroke errors in accordance with Eq. (32).

Command, Control, and Measurement System

A command, control, and measurement computer (CCMC) was developed to command the shape of the model, to implement the control concept, and to facilitate the collection of data. A flow diagram of the system is shown in Fig. 12. The CCMC contains several plug-in boards, including a Texas Instruments digital signal processing (DSP) chip, which is connected to a host 486 microprocessor with the bus used in an IBM PC AT computer. Seventeen Mbytes of memory enables recording time history data of actuator deflections, structural deformations, and commanded voltages at a rate of up to 100 Hz. User-commanded shapes are entered in the microprocessor and are communicated to the DSP for processing. Intensive computations such as the calculation of actuator-stroke error correction commands are performed in the DSP.

Each actuator is controlled by a PMI Motion Technologies motor controller. The motor controller employs pulse-width modulation of a 20-kHz sinusoidal wave such that the controller/actuator

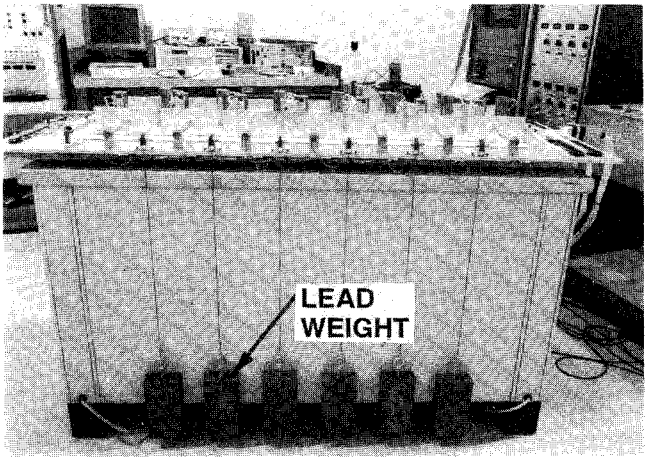

Fig. 8 Lead weights simulating external loads.

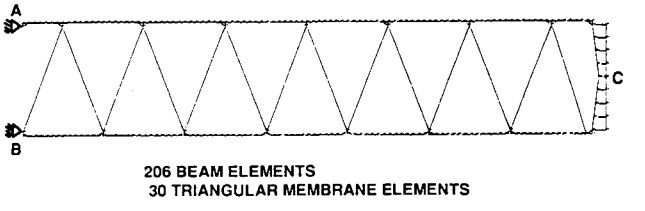

Fig. 9 Finite-element model.

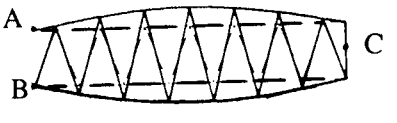

a) Sine/Minus Sine

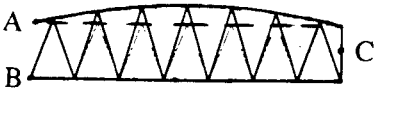

b) Sine/Flat

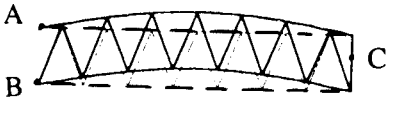

c) Sine/Sine

d) Racking

Fig. 10 Deflections achieved by finite-element analysis.

Table 2 Shape errors for adaptive wing

	Sine/-Sine			Sine/Flat			Sine/Sine			Racking		
		Closed			Closed			Closed			Closed	
	Open	Free	Loaded	Open	Free	Loaded	Open	Free	Loaded	Open	Free	Loaded
1	0.001	0.002	0.001	−0.002	0.002	0.001	−0.002	0.002	0.002	−0.009	0.003	0.008
2	0.021	−0.004	−0.003	0.007	−0.006	−0.005	0.002	−0.006	−0.003	−0.018	−0.003	0.006
3	0.082	−0.003	−0.000	0.060	−0.005	−0.002	0.034	−0.006	0.000	−0.010	−0.003	0.010
4	0.123	0.000	0.005	0.107	−0.002	0.004	0.073	−0.003	0.005	0.018	−0.000	0.016
5	0.126	−0.001	0.004	0.133	−0.004	0.002	0.090	−0.005	0.004	0.018	−0.002	0.014
6	0.056	−0.001	0.005	0.102	−0.004	0.004	0.072	−0.004	0.007	−0.015	−0.004	0.015
7	0.033	0.002	0.007	0.087	−0.003	0.004	0.022	−0.003	0.008	−0.050	−0.004	0.015
8	0.012	−0.001	0.001	0.002	−0.002	−0.002	0.009	−0.003	−0.000	−0.012	−0.000	0.007
9	0.066	−0.002	0.001	0.039	−0.004	−0.003	0.006	−0.006	−0.003	−0.027	−0.002	0.009
10	0.070	0.000	0.005	0.058	−0.002	0.002	0.040	−0.004	0.003	−0.008	−0.000	0.014
11	0.075	−0.006	−0.001	0.087	−0.010	−0.004	0.059	−0.011	−0.002	0.014	−0.008	0.009
12	0.095	−0.002	0.004	0.104	−0.005	0.002	0.058	−0.006	0.004	0.001	−0.004	0.014
13	0.036	0.006	0.011	0.076	0.001	0.008	0.036	−0.001	0.010	−0.029	0.001	0.019
14	0.028	0.001	0.006	0.085	−0.004	0.003	0.003	−0.007	0.004	−0.019	−0.007	0.013

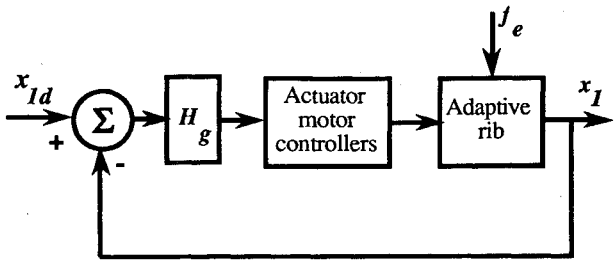

Fig. 11 Diagram of control system.

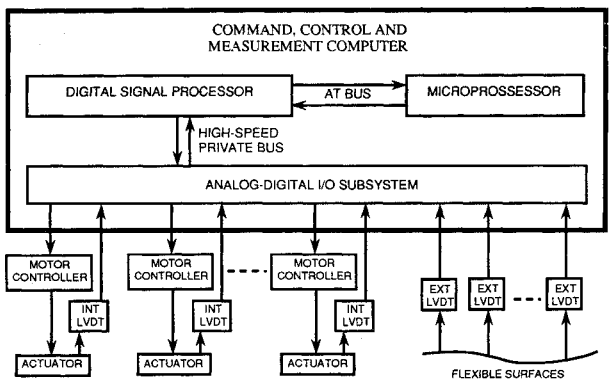

Fig. 12 Command, control, and measurement system architecture.

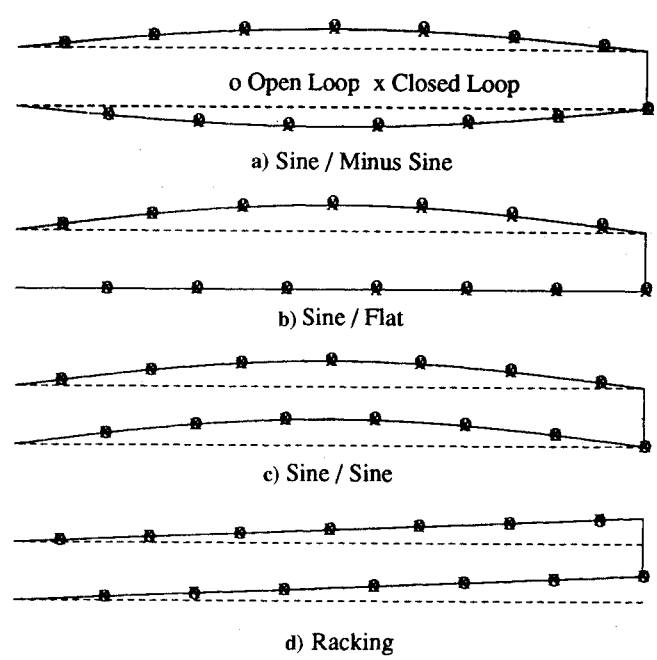

Fig. 13 Test results.

system simulates an ideal proportional position control system where actuator strokes are closely proportional to commanded position-error signals. In this sense, the controllers function as linear amplifiers. Motor-speed regulation provides the necessary damping for stability. Since the motor controllers require analog input and the LVDTs produce analog output, an analog-digital input/output (I/O) subsystem is employed. This system contains analog-to-digital converters and digital-to analog converters, as well as signal-conditioning circuits. Commands are relayed from the DSP to the motor controllers via a direct high-speed private bus and the analog-digital I/O subsystem.

A stress-ratio matrix was developed to predict whether any commanded deformation will result in stresses that are beyond safe allowable values (ultimate stresses with safety factors of 2). When this matrix is multiplied by the vector specifying the desired shape x_1, it provides the ratio of the stresses in each finite element to their allowable values. The matrix resides in the DSP, and the stress computations are performed in real time. If a shape command will result in a stress that is beyond the safe value, the command is automatically scaled down and the operator receives an indication. Also, if unpredicted actuator deflections cause stresses that exceed the allowable safe values, the experiment is automatically shut down. This stress monitoring is accomplished at rates of up to 100 times per sec by measuring the actuator strokes and communicating them to the DSP where the stress ratios are computed. The automatic shutdown is implemented by sending a disable signal to all of the motor controllers to stop all further actuation.

In addition to these safety features, the forces and deflections are limited for each actuator. The force and deflection limits differ for each actuator according to its requirements. The maximum working range of deflection is ±1 in. and of force is ±100 lb. Upper and lower deflection limits are achieved by adjusting the saturation in the preamplifier in each motor controller. Adjustable current limits in the controllers are used to limit the output torques to the motors and thereby limit the output forces of the actuators.

Experimental Results

Open- and closed-loop test results on the free, or unloaded, structure are shown in Fig. 13 for the four shapes shown in Fig. 10. The solid line represents the desired shape, and measured results are shown at each hinge joint. In the sine/minus sine case of Fig. 3a, the amplitude is 0.75 in., whereas in Figs. 3b–3d, the amplitude is 1.0 in.

Errors in the test results are shown in Table 2. Rows 1–7 correspond to points on the upper surface, and rows 8–14 correspond to points on the lower surface, from left to right. Some error analyses have been performed, and we believe that the open-loop errors are mostly attributable to slop in the joints of the structure. Except where the open-loop error is small, with no external loads, the errors are reduced when the loop is closed. When external loads are applied and the loop is open, the errors are very high, on the order of 0.5 in. (not shown in the table); however, they are reduced to reasonable values when the loop is closed (see columns labeled "Load" in Table 2). In the closed-loop case, we believe that the errors are mostly attributable to slop in the joints of the fixtures connecting the LVDTs to the structure. When the external loads are applied, larger actuator torques are required. In this case, the errors increase somewhat because the proportional feedback signal to the actuator motors becomes small as the errors are corrected, thereby limiting the motor torques. We have found that the errors can be reduced somewhat by increasing the gain in the control loop. Studies are recommended to develop lightweight reliable actuators to make wing cross-sectional shape control a reality.

Conclusions

A general method was developed for static shape control of structures with internal actuators. A model of an adaptive rib was constructed, and finite element analysis of the model verifies that the method can provide a close fit to any desired shape that does not overstress the structure. The shape-control method was validated by tests conducted on the model. Commanded shapes were obtained during open-loop control experiments of the unloaded structure and closed-loop experiments of the loaded structure. When applied to the problem of maintaining optimum airfoil shapes during transonic cruise, the method has the potential to significantly reduce wing drag. For the flight conditions investigated, Euler theory demonstrated reductions in the shock-induced wing drag from values ranging from 32 to 68 counts to values of 5 to 10 counts, by small adaptive changes in the wing cross-sectional shape. Studies are recommended to develop lightweight reliable actuators to make wing cross-sectional shape control a reality.

Acknowledgments

The authors gratefully acknowledge the contributions of Christopher C. Tung for finite element studies, Edward Sheedy for mechanical and structural design, Paul V. Aidala and Walter G. Jung for advice on practical aerodynamic considerations, Martin Kesselman for electronic design and analysis, Joseph Su for signal processing, Norman Peele for electrical circuit design and assembly, and Ronald L. Heuer for advice on design and manufacturing.

References

[1]Bonnema, K. L., and Lokos, W. L., "AFTI/F-111 Mission Adaptive Wing Flight Test Instrumentation Overview," *Proceedings of the 35th International Instrumentation Symposium* (Orlando, FL), Instrument Society of America, Research Triangle Park, NC, 1989, pp. 809–840.

[2]Spillman, J. J., "The Use of Variable Camber to Reduce Drag, Weight and Costs of Transport Aircraft," *Aeronautical Journal,* Vol. 96, No. 951, 1992, pp. 1–9.

[3]Austin, F., Rossi, M. J., Jameson, A., Van Nostrand, W., Su, J., and Knowles, G., "Active Rib Experiment for Adaptive Conformal Wing," *Proceedings of the Third International Conference on Adaptive Structures* (San Diego, CA), Technomic Publishing, Lancaster, PA, 1992, pp. 43–55.

[4]Austin, F., Van Nostrand, W., and Rossi, M. J., "Shape Control of Structures with Semi-Definite Stiffness Matrices for Adaptive Wings," *Proceedings of the Smart Structures and Materials 1993, Smart Structures and Intelligent Systems* (Albuquerque, NM), Vol. 1917, SPIE, Bellingham, WA, 1993, pp. 419–425.

[5]Rossi, M., Austin, F., and Van Nostrand, W., "Active Rib Experiment for Shape Control of an Adaptive Wing," *Proceedings of the AIAA/ASME/ASCE/AHS/ASC 34th Structures, Structural Dynamics, and Materials Conference,* AIAA, Washington, DC, 1993, pp. 3485–3489 (AIAA Paper 93-1700).

[6]Stewart, G. W., *Introduction to Matrix Computations,* 1st ed., Academic Press, San Diego, CA, 1973, pp. 317–325.

[7]Jameson, A., "Aerodynamic Design Via Control Theory," *Journal of Scientific Computing,* Vol. 3, No. 3, 1988, pp. 233–260.

[8]Jameson, A., "Automatic Design of Transonic Airfoils to Reduce Shock Induced Pressure Drag," Princeton Univ. Rept. MAE 1881, Princeton, NJ, Feb. 1990; also *Proceedings of the 31st Israel Annual Conference on Aviation and Aeronautics* (Tel Aviv), Technion, Haifa, Israel, 1990, pp. 5–17.